PREGNANCY



# Integrated trajectories of the maternal metabolome, proteome, and immunome predict labor onset

Ina A. Stelzer[1†], Mohammad S. Ghaemi[1,2†], Xiaoyuan Han[1,3†], Kazuo Ando[1†], Julien J. Hédou[1†], Dorien Feyaerts[1], Laura S. Peterson[4], Kristen K. Rumer[1], Eileen S. Tsai[1], Edward A. Ganio[1], Dyani K. Gaudillière[5], Amy S. Tsai[1], Benjamin Choisy[1], Lea P. Gaigne[1], Franck Verdonk[1], Danielle Jacobsen[1], Sonia Gavasso[1,6], Gavin M. Traber[7], Mathew Ellenberger[7], Natalie Stanley[1,8], Martin Becker[1,8], Anthony Culos[1,8], Ramin Fallahzadeh[1,8], Ronald J. Wong[4], Gary L. Darmstadt[9], Maurice L. Druzin[10], Virginia D. Winn[11], Ronald S. Gibbs[10], Xuefeng B. Ling[12], Karl Sylvester[12], Brendan Carvalho[1], Michael P. Snyder[7], Gary M. Shaw[4], David K. Stevenson[4], Kévin Contrepois[7], Martin S. Angst[1‡], Nima Aghaeepour[1,4,8‡], Brice Gaudillière[1,4,*‡]

**Estimating the time of delivery is of high clinical importance because pre- and postterm deviations are associated with complications for the mother and her offspring. However, current estimations are inaccurate. As pregnancy progresses toward labor, major transitions occur in fetomaternal immune, metabolic, and endocrine systems that culminate in birth. The comprehensive characterization of maternal biology that precedes labor is key to understanding these physiological transitions and identifying predictive biomarkers of delivery. Here, a longitudinal study was conducted in 63 women who went into labor spontaneously. More than 7000 plasma analytes and peripheral immune cell responses were analyzed using untargeted mass spectrometry, aptamer-based proteomic technology, and single-cell mass cytometry in serial blood samples collected during the last 100 days of pregnancy. The high-dimensional dataset was integrated into a multiomic model that predicted the time to spontaneous labor [$R = 0.85$, 95% confidence interval (CI) [0.79 to 0.89], $P = 1.2 \times 10^{-40}$, $N = 53$, training set; $R = 0.81$, 95% CI [0.61 to 0.91], $P = 3.9 \times 10^{-7}$, $N = 10$, independent test set]. Coordinated alterations in maternal metabolome, proteome, and immunome marked a molecular shift from pregnancy maintenance to prelabor biology 2 to 4 weeks before delivery. A surge in steroid hormone metabolites and interleukin-1 receptor type 4 that preceded labor coincided with a switch from immune activation to regulation of inflammatory responses. Our study lays the groundwork for developing blood-based methods for predicting the day of labor, anchored in mechanisms shared in preterm and term pregnancies.**

## INTRODUCTION

During human pregnancy, the onset of labor is precisely timed to ensure the delivery of a healthy newborn. However, what determines the timing of parturition is not clearly understood. The ability to accurately predict the timing of labor is of high clinical importance because preterm (<37 weeks of gestation) or postterm (>42 weeks of gestation) deviations are associated with complications for the mother and her offspring (*1*, *2*).

Existing methods for predicting the day of labor perform poorly (*3*–*5*). In current clinical practice, the estimate day of delivery (EDD) is calculated on the basis of the first day of the last menstrual period (LMP) and assumes a gestational length of 40 weeks (*6*, *7*). The gestational age (GA) and EDD are further determined by the first accurate ultrasound examination (*8*). Although they are useful for managing the pregnancy, the EDD and GA are not accurate predictors for when labor will actually occur because most pregnancies deviate from the norm of 40 weeks of gestational duration. To advance clinical decision-making, further estimation approaches including predictive biomarkers are critically needed to better predict the actual labor onset, leading to delivery in healthy and pathological pregnancies.

A comprehensive characterization of the biological processes that precede spontaneous labor is a key step for the identification of predictive biomarkers. The maintenance of pregnancy relies on finely tuned adaptations (*9*–*11*), which are readily detectable in maternal blood using high-content metabolomic, proteomic, and single-cell cytometric technologies (*12*–*17*). At the onset of labor, a major transition occurs in the fetomaternal physiology that culminates in the delivery of the fetus, including the breakdown of fetomaternal immune tolerance by immune infiltration into fetal membranes and the placenta (*18*, *19*), endocrine changes (*20*, *21*), rupture of fetal membranes (*22*), cervical dilation, and augmentation of uterine contractility (*23*).

The timing of systemic molecular and cellular events that mark the transition from pregnancy maintenance to parturition, which begins with labor contractions and/or spontaneous rupture of membranes

[1]Department of Anesthesiology, Perioperative and Pain Medicine, Stanford University School of Medicine, Palo Alto, CA 94305, USA. [2]Digital Technologies Research Centre, National Research Council Canada, Toronto, ON M5T 3J1, Canada. [3]Department of Biomedical Sciences, University of the Pacific, Arthur A. Dugoni School of Dentistry, San Francisco, CA 94103, USA. [4]Division of Neonatal and Developmental Medicine, Department of Pediatrics, Stanford University School of Medicine, Palo Alto, CA 94305, USA. [5]Division of Plastic and Reconstructive Surgery, Department of Surgery, Stanford University School of Medicine, Palo Alto, CA 94305, USA. [6]Department of Neurology, NeuroSys-Med, Haukeland University Hospital, 5021 Bergen, Norway. [7]Department of Genetics, Stanford University School of Medicine, Palo Alto, CA 94305, USA. [8]Department of Biomedical Data Science, Stanford University School of Medicine, Palo Alto, CA 94305, USA. [9]Division of Neonatology, Department of Pediatrics, Stanford University School of Medicine, Palo Alto, CA 94305, USA. [10]Division of Maternal Fetal Medicine, Department of Obstetrics and Gynecology, Stanford University School of Medicine, Palo Alto, CA 94305, USA. [11]Department of Obstetrics and Gynecology, Stanford University School of Medicine, Palo Alto, CA 94305, USA. [12]Department of Surgery, Stanford University School of Medicine, Palo Alto, CA 94305, USA.
*Corresponding author. Email: gbrice@stanford.edu
†These authors contributed equally to this work as co–first authors.
‡These authors contributed equally to this work as co–last authors.

(*24*), is ill-defined. Prior studies have provided important information with regard to systemic maternal adaptations that track GA during pregnancy (*13*, *15*–*17*, *25*). However, to understand the biological transition to labor, studies are needed that specifically examine labor biology in relation to spontaneous labor onset, rather than in relation to the estimated GA. Limitations in either study design, such as inclusion of medically induced labor cases, or technology, such as the limited coverage of immune system–wide adaptations, have precluded a comprehensive analysis of biologic events preceding spontaneous labor and delivery.

In this study, we combined an untargeted mass spectrometry approach (*26*) with an aptamer-based technology (*27*) to quantify the concentrations of 4846 metabolomic and proteomic analytes in longitudinally collected plasma samples during the 100-day period preceding spontaneous labor onset. In parallel, we used a single-cell mass cytometry immunoassay to quantify the dynamic changes in the distribution and intracellular signaling responses of all major innate and adaptive peripheral immune cells (2296 features). The analysis generated three high-dimensional omic datasets. We applied a stacked generalization (SG) algorithm to the multiomic dataset to build and independently validate an integrated model that predicted the time to labor (TL). Model component trajectories revealed precisely timed alterations that marked a transition from pregnancy maintenance to prelabor biology. Our findings and predictive modeling approach can serve to identify elements of a common pathway that precedes labor in term as well as pre- or postterm pregnancies.

## RESULTS

### Maternal metabolome, proteome, and immunome are assessed in the 100 days preceding the day of labor

One-hundred twelve pregnant women receiving routine antepartum care at the Lucile Packard Children's Hospital in Stanford, CA, USA, were enrolled during their second or third trimester of pregnancy. After exclusion of patients who did not meet the inclusion criteria, such as medical induction of labor (see Materials and Methods), an analysis was performed on samples from 53 patients (training cohort) with spontaneous labor contractions. The day of labor for this study is defined as the day of admission for spontaneous labor (contractions occurring at least every 5 min, lasting >1 min, and associated with cervical change). All patients in the training cohort were in stage I labor on the day of labor at the time of diagnosis, among which 73.6% were in the latent phase and delivered within 11 hours [interquartile range (IQR) [5, 18] hours]. The remaining 26.4% were in the active phase of labor and delivered within 4 hours (IQR [2, 10] hours). The difference between the day of labor and day of delivery ranged from 0 to 1 day (median = 0; SD = 0.23; range [0, 1] days). Five women in the training cohort delivered preterm [34 weeks + 0 days (34+0) to <37 weeks of gestation]. An independent analysis was performed on samples from 10 additional patients (test cohort), who had spontaneous labor ($N$ = 5) or spontaneous rupture of membranes ($N$ = 5). Patient demographics including labor and delivery, as well as ante- and peripartum parameters are shown in Table 1.

For each study participant, serial blood samples [median of three samples (plasma and whole blood) per patient, range [1, 3]] were collected during the last 100 days before labor (Fig. 1A). The approach leveraged the interindividual variabilities in sample collection time to define a continuous variable, the TL, which describes the difference between the day of sampling and the day of labor. In the aggregated sample cohort of all patients, the TL was distributed with near daily resolution across the last 100 days of pregnancy with a median time of blood sampling of 36 days (~5 weeks) before the day of labor. The plasma concentration of 3529 metabolites and 1317 proteins were quantified using a high-throughput untargeted mass spectrometry and an aptamer-based proteomic platform, respectively (Fig. 1B). Using a 46-parameter mass cytometry assay (table S1), a total of 2296 single-cell immune features were extracted from each sample including the frequencies of 41 immune cell subsets, representing major innate and adaptive populations, endogenous intracellular activities such as phosphorylation states of 11 signaling proteins, and capacities of each cell subset to respond to a series of receptor-specific immune challenges [lipopolysaccharide (LPS), interferon-α (IFN-α), granulocyte-macrophage colony-stimulating factor (GM-CSF), and a combination of interleukin-2 (IL-2), IL-4, and IL-6].

### Multiomic modeling of the maternal interactome predicts labor onset

The combined metabolome, proteome, and immunome datasets produced 7142 features per sample. Features were visualized with three correlation networks, highlighting intraomic (within-dataset) correlations across the last 100 days before the day of labor (Fig. 2, A to C). A single chord diagram highlighted interomic (between-dataset) correlations between features from two different datasets (Fig. 2, D and E), after controlling to a false discovery rate (FDR) of 0.05 (Spearman $R > 0.46$) computed from the distribution of correlation between randomly generated features (Fig. 2D). Individual biological systems were tightly orchestrated because 99% of all omic correlations were found in feature pairs belonging to the same dataset (Fig. 2, A to C).

Correlations between the three biological systems included 3995 weak ($R$ = 0.46 to 0.59), 596 moderate ($R$ = 0.6 to 0.79), and 21 strong ($R$ = 0.8 to 1.0) interomic correlations (Fig. 2, E and F), revealing an interactome of late pregnancy. Of all interomic correlations ($R > 0.46$, FDR < 0.05), 80% were observed between the metabolome and proteome, 4% between the immunome and proteome, and 16% between the immunome and metabolome (Fig. 2F). Overall, the multimodal analysis of plasma analytes and peripheral blood immune cells measured during pregnancy revealed a concerted behavior between the metabolomic, proteomic, and immunologic systems. The interactome analysis did not account for the timing of omic measurements, such that observed correlations were not enriched for interactions temporally linked to the time in pregnancy. However, the analysis highlighted the interconnected nature of the multiomic dataset, justifying the need for an integrated approach to identify biologically relevant components predictive of the TL.

Peripheral blood metabolic, proteomic, and immunologic events informed an integrated approach to predict the TL. Here, multivariate least absolute shrinkage and selection operator (LASSO) linear regression models were first individually built for each omic dataset and then integrated into a single model by SG. An advantage of the SG method is that differences in size and modularity of individual omic modalities are accounted for to prevent datasets of higher dimensions (such as the metabolome) to overwhelm the integrated model (Fig. 3A) (*14*, *28*). The SG model predicted the TL from the measurement of metabolic, proteomic, and immunologic features with high accuracy [$R$ = 0.85, 95% confidence interval (CI) [0.79 to 0.89], $P = 1.2 \times 10^{-40}$, root mean square error (RMSE) = 17.7 days,

**Table 1. Pregnancy cohort demographics.** N/A, not applicable.

| Pregnancy characteristics | Training cohort | | Test cohort | |
|---|---|---|---|---|
| | *N* = 53<br>*n* = 150 | Percentage or median [interquartile range] | *N* = 10<br>*n* = 27 | Percentage or median [interquartile range] |
| Age (years) | 53 | 33 [30, 35] | 10 | 31 [29, 33] |
| Body mass index (BMI) first trimester (kg/m$^2$) | 46 | 23.4 [21.1, 25.6] | 6 | 24.3 [20.7, 25.3] |
| BMI third trimester (kg/m$^2$) | 46 | 27.6 [24.8, 30.1] | 10 | 26.3 [23.5, 27.7] |
| Gestational age (GA) at delivery, all (weeks) | 53 | 39.4 [38.8, 40.0] | 10 | 39.3 [38.7, 40.3] |
| Preterm delivery (<37 weeks) | 5 | 9.4% | 0 | N/A |
| GA at delivery, preterm (weeks) | 5 | 34.3 [34.0, 35.3] | 0 | N/A |
| Gravidity | 53 | 2.0 [1.0, 3.0] | 10 | 1.7 [1.0, 2.0] |
| Parity (% nulliparous) | 30 | 56.6% | 6 | 60% |
| Infant sex | 23 | Female (43.4%) | 2 | Female (20%) |
| Birth weight (g) | 52 | 3238 [2983, 3685] | 10 | 3483 [3155, 3880] |
| 5-min Apgar score | 52 | 9 [9, 9] | 9 | 8.8 [9, 9] |
| **Race** | | | | |
| East Asian | 16 | 30.2% | 6 | 60% |
| South Asian | 7 | 13.2% | 0 | 0% |
| Southeast Asian | 3 | 5.7% | 0 | 0% |
| African-American | 0 | 0% | 0 | 0% |
| Native Hawaiian/Pacific Islander | 1 | 1.9% | 0 | 0% |
| Middle Eastern | 1 | 1.9% | 0 | 0% |
| White | 19 | 35.9% | 3 | 30% |
| Two or more races | 2 | 3.8% | 0 | 0% |
| Other | 4 | 7.6% | 1 | 10% |
| **Ethnicity** | | | | |
| Hispanic | 2 | 3.8% | 0 | 0% |
| Non-Hispanic | 51 | 96.2% | 10 | 100% |
| **Labor and delivery** | | | | |
| Time to labor (TL) at sampling, all (days) | 53 | −36 [−71, −15] | 10 | −33 [−49, −17] |
| TL at sampling, preterm (days) | 5 | −24 [−48, −14] | 0 | N/A |
| Spontaneous rupture of membranes | 53 | 100% | 10 | 100% |
| Spontaneous onset of labor | 53 | 100% | 5 | 50% |
| Vaginal | 48 | 90.6% | 7 | 70% |
| Cesarean section during labor | 5 | 9.4% | 3 | 30% |
| **Comorbidity** | | | | |
| Gestational diabetes | 4 | 7.6% | 0 | 0% |
| Polycystic ovary syndrome | 1 | 1.9% | 0 | 0% |
| Gestational hypertension | 4 | 7.6% | 0 | 0% |
| Preeclampsia | 3 | 5.7% | 0 | 0% |
| History of preterm birth | 6 | 11.3% | 0 | 0% |
| Progesterone treatment | 3 | 5.7% | 0 | 0% |

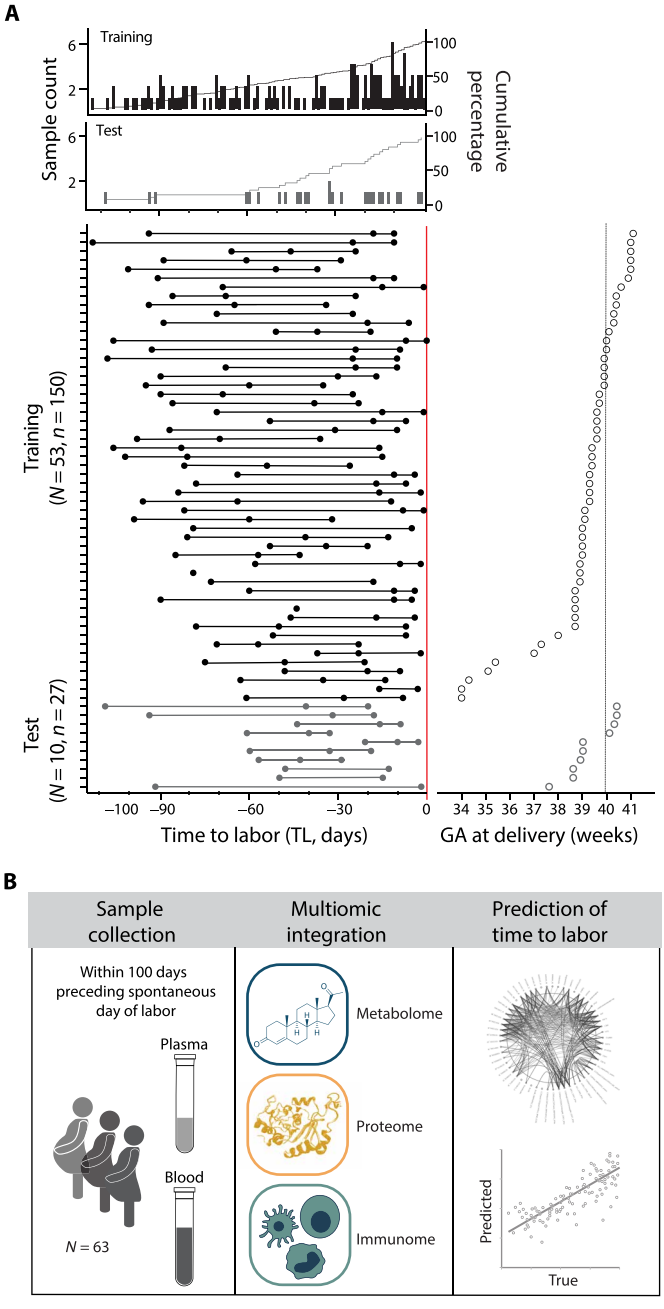


**Fig. 1. The maternal metabolome, proteome, and immunome were assessed during the 100-day period preceding the day of labor.** (**A**) Peripheral blood was obtained serially from 63 women during the 100 days preceding spontaneous labor. The primary outcome of the analysis was the time to labor (TL), such that the prediction of the day of labor did not consider estimates of GA. Raster plots depicting the day of sampling for the training (top plot; $N = 53$, $n = 150$ samples) and test (bottom plot; $N = 10$, $n = 27$ samples) cohort, and the TL distribution (range [-112, 0]), calculated as the difference between the day of labor (TL 0, red line) and the day of sampling (filled dots). At least one sample was collected on any day of the 100 days preceding the day of labor (cumulative count plot). (**B**) Plasma samples were used in the analysis of the circulating metabolome (high-throughput mass spectrometry) and proteome (aptamer-based technology). Whole-blood samples were used in the analysis of the systemic immunome (mass cytometry). In total, 7142 features were generated per sample from all three datasets and integrated into a multivariate model to predict the TL.

$N = 53$] (Fig. 3B). Statistical significance was established using a cross-validation method that accounts for the high dimensionality of the data. The generalizability of the SG model was prospectively tested in an independent cohort of 10 additional women ($R = 0.81$, 95% CI [0.61 to 0.91], $P = 3.9 \times 10^{-7}$, RMSE = 17.4 days) (Fig. 3C).

Five of the 53 patients included in the training cohort experienced spontaneous preterm labor (GA at delivery < 37 weeks). Although comparing term and preterm labor was not a primary aim of the study, the presence of these five patients questioned whether the integrated SG approach would generalize to predict the TL when labor occurred preterm. A new model trained on a subcohort of patients with term labor successfully predicted the TL for patients with preterm labor ($R = 0.67$, 95% CI [0.21 to 0.86], $P = 8.8 \times 10^{-3}$, RMSE = 27.3 days; fig. S1, A to D). In addition, there was a strong overlap between the most informative features of the original model (including term and preterm patients) and the term-only model (fig. S1, E to G; $R = 0.68$ to 0.78, Spearman correlation in bootstrap feature ranking between the two models). The results suggest that the SG model generalized to the prediction of the TL for both term and preterm labor. The data also confirm that the SG model built on the entire patient cohort was not driven by a preterm-specific prelabor biology. A confounder analysis further established that the prediction accuracy was not influenced by other clinical or demographic variables [including race, body mass index (BMI), and major comorbidities; table S2]. In summary, our assessment of maternal circulating factors in the peripheral blood provided an accurate prediction for the timing of labor that was independent of the GA based on EDD.

## Trajectories of metabolome, proteome, and immunome reveal alterations in prelabor dynamics

To facilitate the biological interpretation of the multivariate SG model, we focused on the model features that contributed most to the prediction of the TL (selected using a bootstrap and ranking approach; see Materials and Methods). These features included 12 metabolomic, 18 proteomic, and 15 immune cell features (Fig. 3D and table S3) and formed a correlation network that segregated into two clusters (Fig. 3E). For each cluster, enriched proteomic and metabolomic pathways were identified using the Fisher's test (*29*) and the hypergeometric test (*30*), respectively. The lower cluster was enriched for metabolic features representing steroid hormone biosynthesis, and pentose and glucuronate interconversions (carbohydrate metabolism) that clustered with innate and adaptive immune cell responses to IFN-α stimulation [including phosphorylated signal transducer and activator of transcription 1 (pSTAT1) and phosphorylated mitogen-activated protein kinase–activated protein kinase (pMK2) in dendritic cells (DCs), natural killer (NK) cells, and T cell subsets] (Fig. 3E). The upper cluster contained metabolic features enriched for tryptophan metabolism and proteins representing glycoprotein metabolic pathways that clustered with various immune cell features, including granulocyte frequencies, signaling responses to GM-CSF in nonclassical monocytes (ncMCs) and basal pMK2 signaling in T cell subsets (Fig. 3E).

The pathway enrichment analysis provided a snapshot of key biological systems temporally linked to the TL. To examine the dynamic behavior of biological events predictive of the TL, individual model features were plotted over time (Fig. 4, figs. S2 to S4, and table S3). Classifying the dynamic behavior of each feature revealed three general trajectory patterns on the basis of the goodness of fit of a pattern-fitting model (Fig. 4A and table S4): linear progression

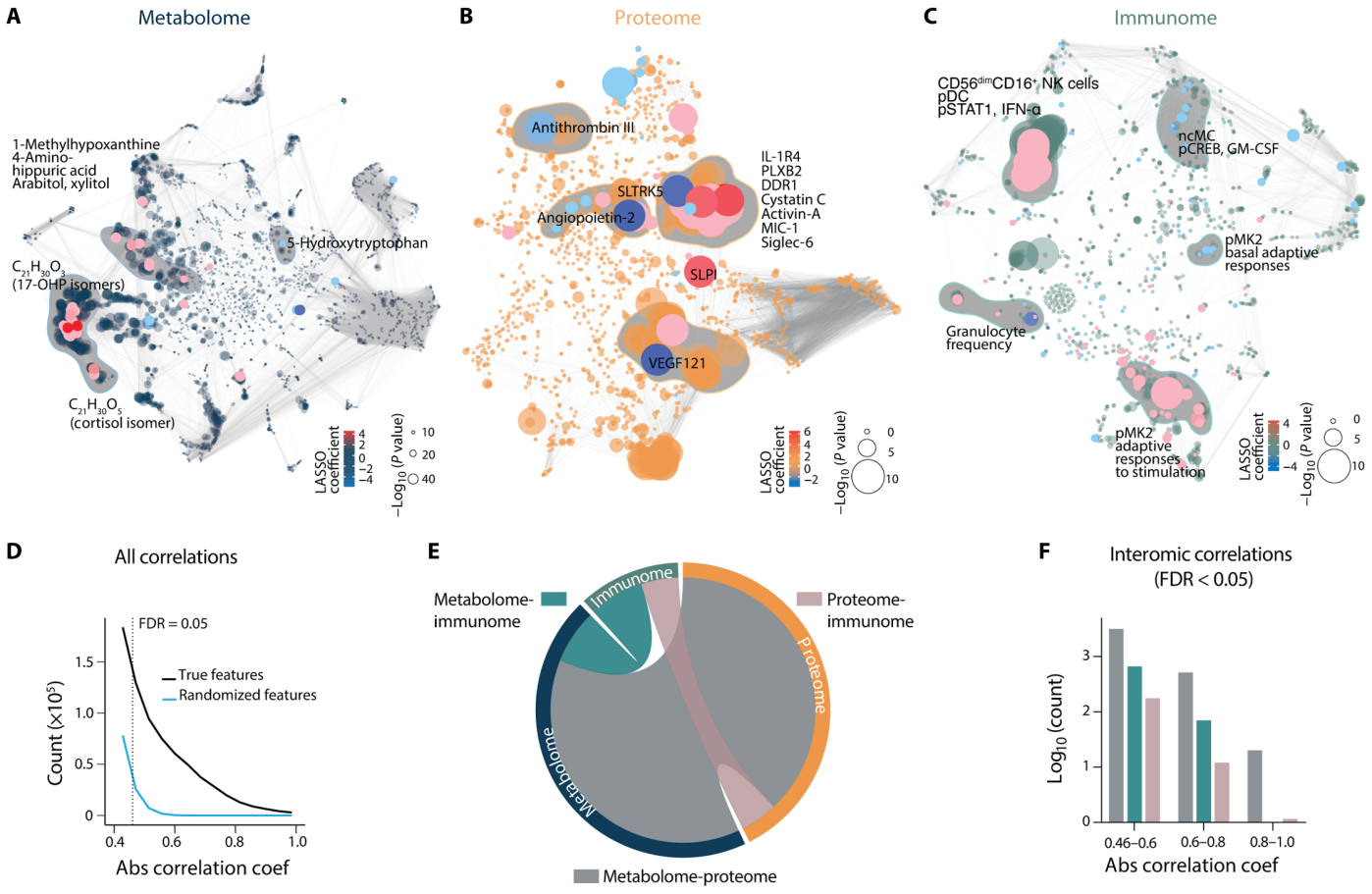


**Fig. 2. The late-gestational maternal interactome highlights interconnectivity between biological systems.** (**A** to **C**) Intraomic correlation networks of metabolome, proteome, and immunome features during the 100 days preceding labor in the training cohort ($N = 53$). Each node represents a biological feature. Correlations between features are represented by edges. Red/blue nodes highlight features positively/negatively correlated with the TL. Dot size indicates the $-\log_{10}$ of $P$ value of the correlation (Spearman). Clusters of features most highly correlated with the TL are shaded in gray and annotated. (**D**) Distributions of all correlations within (intraomic) and between (interomic) modalities in the original as well as simulated random datasets. The false discovery rate (FDR) threshold of 0.05 was computed from the generated distribution of random features in a target-to-decoy approach to filter the correlations with FDR > 0.05, corresponding to an absolute ($|x|$) correlation coefficient cutoff at 0.46. (**E**) Chord diagram of interomic (between-dataset) correlations between metabolome, proteome, and immunome features in the last 100 days before the day of labor. The outer circle represents all features with FDR-adjusted absolute correlation coefficients [Spearman $R$ (0.46, 1.0), FDR < 0.05], colored by the respective biological modality. Shaded inner connections represent interomic correlations between the metabolome, proteome, and immunome as specified by color codes. The number of FDR-adjusted interactions between two omics is visualized as normalized to the number of total possible interomic interactions. (**F**) Quantification of the number of interomic interactions visualized in (E). The number of interomic correlations between the three biological modalities divided into weak (0.46 to 0.6), moderate (0.6 to 0.8), and strong (0.8 to 1.0) absolute correlation coefficients is shown.

(degree 1; Fig. 4, B to D) or quadratic progression, including accelerating (surging of an increasing or decreasing pattern over time) (degree 2a; Fig. 4, E to G) or decelerating (plateauing of an increasing or decreasing pattern over time) (degree 2b; Fig. 4, H to J) progression (table S4). We plotted the distribution of trajectory patterns across all datasets. The resulting plot (Fig. 4K) showed a remarkable overlap of the behavior of metabolomic and proteomic model features, which were predominantly classified as degree 1 (constant rate). In contrast, immune cell trajectories predominantly followed a degree 2b (decelerating) pattern.

Degree 1 trajectories highlighted biological processes progressing linearly throughout the last 100 days of pregnancy until labor (Fig. 4, B to D). For example, the plasma concentration of an isomer of cortisol, strongly correlating with cortisol (Spearman $R = 0.7$; Materials and Methods), increased steadily from TL −100 to labor onset (Fig. 4B), recapitulating known steroid changes occurring throughout pregnancy (*31*, *32*). Similarly, proteins expressed by fetal membranes constantly increased throughout the 100 days before labor, such as plexin-B2 (PLXB2) (*33*) and discoidin domain receptor-1 (DDR1) (fig. S3) (*34*). In contrast, Angiopoietin-2, a protein that contributes to placental vascular development, decreased at a constant rate throughout the study period (Fig. 4C) (*35*, *36*). In addition to the many proteomic and metabolomic model features with constant pattern trajectories, accelerating (degree 2a) or decelerating (degree 2b) trajectories denoted important prelabor alterations of the maternal metabolome and proteome (Fig. 4, E, F, H, and I).

Among the most informative degree 2 metabolomic features were isomers of 17-hydroxyprogesterone (17-OHP) and 17-hydroxypregnenolone sulfate, an upstream substrate for the production of 17-OHP. The isomers of 17-OHP correlate with 17-OHP,

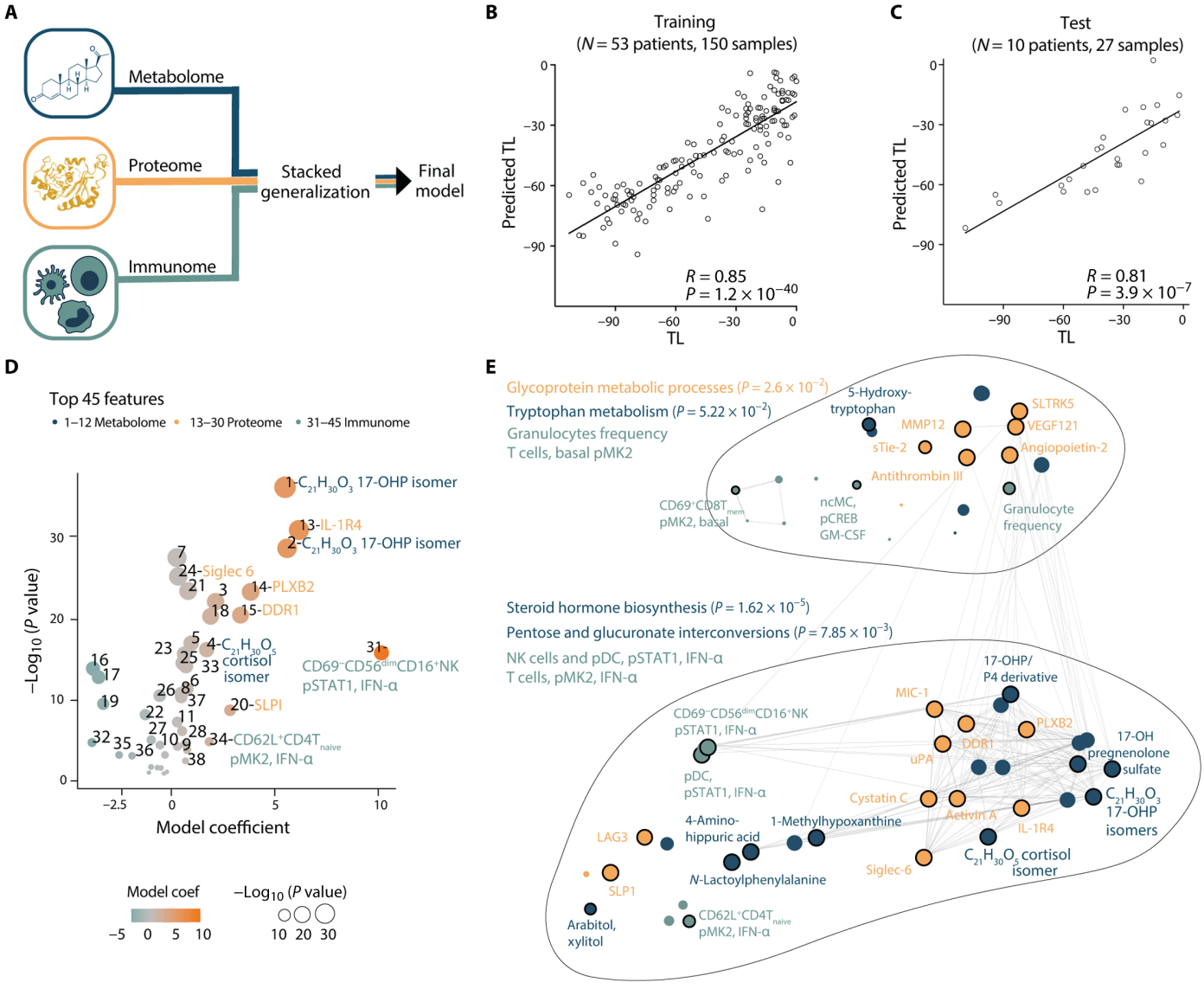


**Fig. 3. Multiomic modeling of the maternal interactome predicts labor onset.** (**A**) Integration of all three modalities (metabolome, proteome, and immunome) using a stacked generalization (SG) method. (**B** and **C**) Regression of predicted versus true TL (days) derived from the SG model [training cohort, Pearson $R = 0.85$, 95% CI [0.79 to 0.89], $P = 1.2 \times 10^{-40}$, RMSE = 17.7 days, $N = 53$ patients (B); test cohort, Pearson $R = 0.81$, 95% CI [0.61 to 0.91], $P = 3.9 \times 10^{-7}$, RMSE = 17.4 days, $N = 10$ patients (C)]. (**D**) Volcano plot depicting the 45 most informative SG model features in the training cohort. Feature importance to the overall predictive model is plotted on the *x* axis (SG model coefficient), correlation with the TL is plotted on the *y* axis [$-\text{Log}_{10}$ (*P* value)]. Orange colors depict positive correlations with the TL, and teal colors depict negative correlations. See table S3 for number-to-feature key. (**E**) Pathway enrichment analysis was performed on metabolic and proteomic top SG model features (see Materials and Methods; *P* values derived from hypergeometric and Fisher's test). All 45 most informative model features are depicted in a correlation network to visualize interomic correlations (edges indicate an absolute $R > 0.46$, $N = 53$). See also Fig. 4, fig. S1, and table S3.

suggesting that they have similar biological functions and belong to similar pathways (Materials and Methods). Plasma concentrations of these features increased in accelerated fashion within the last 30 days before the day of labor (Fig. 4E and fig. S2). Whereas this finding confirms known progesterone biology in the late third trimester (*37*, *38*), our data provide additional temporal information showing that a surge in 17-OHP, one of the most informative features of the predictive model, is tightly linked to the timing of labor. Furthermore, metabolites with degree 2b trajectories included pregnenolone sulfate (*39*), which showed decelerating behavior, stagnating around 30 days before the day of labor (Fig. 4H).

Among the most informative degree 2 proteomic features of the predictive model were trajectories whose accelerating or decelerating patterns pointed toward important prelabor alterations in placental biology, coagulation, and inflammation. The most informative degree 2a proteomic feature was IL-1 receptor type 4 (IL-1R4), the soluble inhibitory receptor of the proinflammatory cytokine IL-33. IL-1R4 plasma concentration surged during the last 30 days before labor (Fig. 4F and fig. S3). The data complement prior studies showing an elevated concentration of IL-1R4 during the third trimester of pregnancy (*40*, *41*). Surging concentrations of IL-1R4 observed in the systemic circulation may counteract the proinflammatory

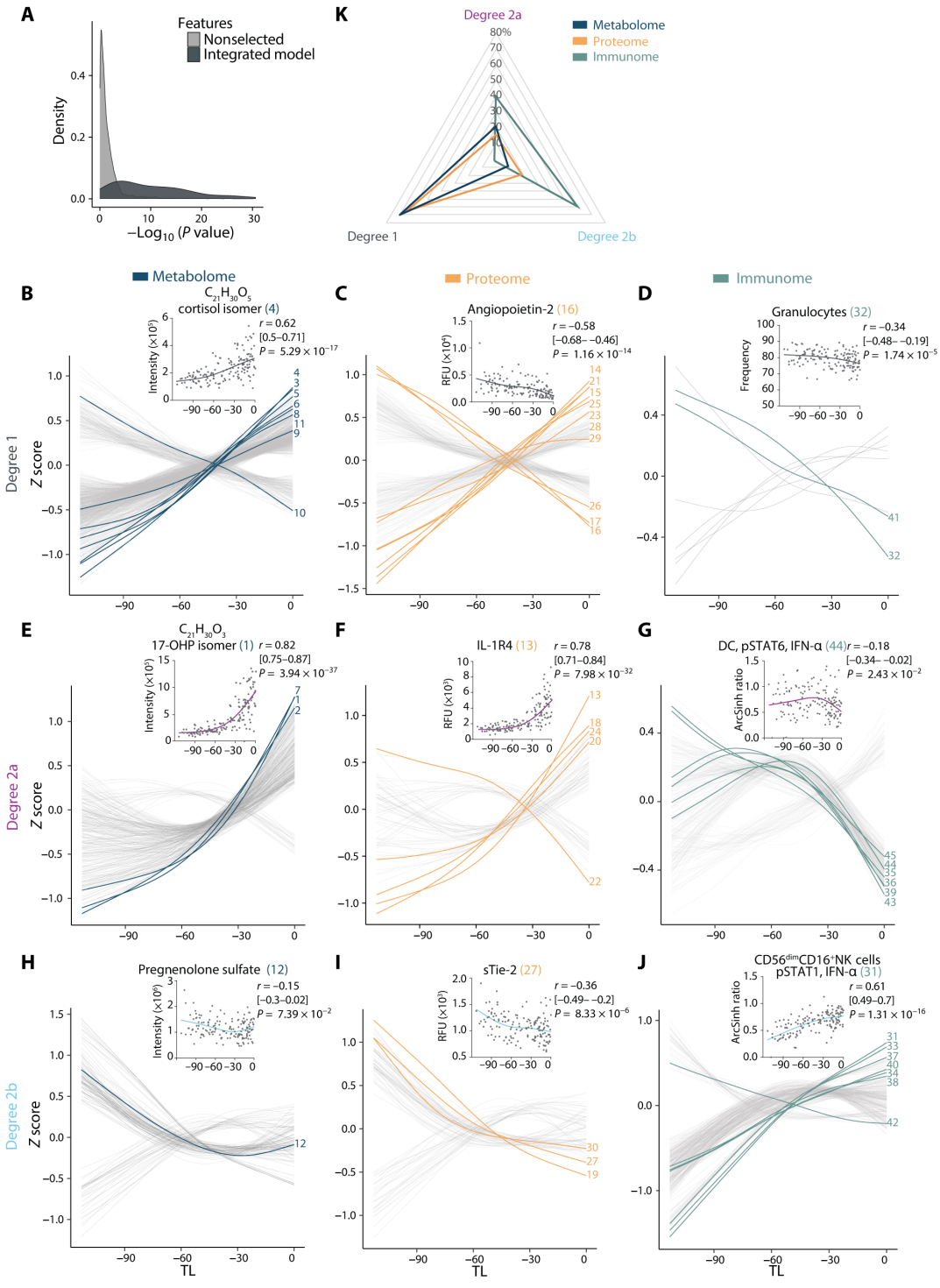


**Fig. 4. Trajectories of the maternal metabolome, proteome, and immunome reveal alterations in prelabor dynamics.** (**A**) Distribution of relevance-of-fit *P* values for the trajectories assigned to SG model features in comparison to nonselected features demonstrates goodness of fit of curve classification ($N = 53$ patients, $n = 150$ samples). Feature trajectories were classified as linear or quadratic on the basis of the goodness of fit with Akaike information criterion and relevance of fit with associated *P* value (*F* statistic). Degree 1 (**B** to **D**), degree 2a (**E** to **G**), or degree 2b (**H** to **J**) trajectories are plotted over time for the metabolome (left), proteome (middle), and immunome (right). Lines represent smoothened spline (df = 3, *Z*-scored) for all features. The most informative model features are highlighted and numbered (in reference to Fig. 3D and table S3). A representative feature is shown (inset) for each trajectory type including its correlation with TL (Spearman coefficient [95% CI], and associated *P* value). (**K**) Radar plot quantifying the distribution of degree 1 (linear), degree 2a [quadratic, accelerating (surging of an increasing or decreasing pattern over time)], and degree 2b [quadratic, decelerating (plateauing of an increasing or decreasing pattern over time)] trajectories among all multiomic features. See also figs. S2 to S6 and tables S3 and S4.

effects of IL-33, potentially released upon mechanical uterine distension and in the context of the local inflammation occurring at the fetomaternal interface (*42*, *43*). Hence, IL-1R4 may be an important regulator of inflammation during the late phase of pregnancy.

Also surging with approaching labor (degree 2a) were two proteins highly expressed by the placenta, Activin-A and sialic acid binding immunoglobulin-like lectin–6 (Siglec-6) (fig. S3). In contrast, the trajectory of antithrombin III (ATIII), an endogenous anticoagulant (*44*), negatively accelerated during the last 30 days before the day of labor (fig. S3). Soluble tunica interna endothelial cell kinase–2 (sTie-2), a regulator of angiopoietin availability for vasculogenesis (*45*), displayed a decelerating trajectory (Fig. 4I). Overall, together with the constantly rising concentrations of fetal membrane–derived PLXB2 and DDR1 (fig. S3), the coordinated trajectories of angiogenic factors sTie-2, Angiopoietin-2 (Fig. 4C), and vascular endothelial growth factor 121 (VEGF121) as well as Activin-A, and Siglec-6 (fig. S3) suggest that these proteins are integral components of a plasma fetoplacental signature that portends the impending day of labor.

Plasma metabolites and proteins form the interactive environment for circulating immune cells. Immune cell trajectories predominantly followed a decelerating pattern (Fig. 4, D, G, and J), in contrast to

accelerating or constantly increasing plasma analyte trajectories (Fig. 4K). Granulocyte frequencies decreased over time (Fig. 4D). In parallel, decelerating signaling trajectories were observed along the Janus kinase (JAK)–STAT and myeloid differentiation primary response 88 (MyD88) signaling pathways in both innate and adaptive immune cells (fig. S4). This decelerating behavior was particularly pronounced in innate immune cells, as illustrated by the pSTAT1 signal in $CD56^{dim}CD16^{+}$ NK cells and the pSTAT6 signal in DCs in response to IFN-α (Fig. 4, G and J), the phosphorylated cyclic adenosine monophosphate response element–binding protein (pCREB) response in ncMCs in response to GM-CSF (fig. S4), and the phosphorylated P38 mitogen-activated protein kinase (pP38), phosphorylated extracellular signal–regulated kinase (pERK) and pCREB signals in classical monocytes (cMCs) in response to LPS and GM-CSF (fig. S5). During the 100 days preceding labor, proinflammatory innate immune cell responses first increased, in accordance with their previously described trajectory during the first and second trimesters (*12*), and then stagnated or decreased closer to the day of labor. These findings indicate a regulated dampening of systemic immune cell responses before the day of labor that may counterbalance the local inflammatory environment emerging at the fetal membranes, cervix, and fetomaternal interface during labor and parturition (*46*).

### A breakpoint defined by nonlinearity of omic trajectories demarcates a transition from pregnancy to prelabor biological adaptations

The presence of degree 2 (quadratic) trajectories across all omic datasets pointed toward a period of disruption with approaching labor that resonated across all measured biological systems (Fig. 4, E to J). Identifying the timing of such a nonlinear transition is clinically relevant because it defines when the assessment of peripheral blood analytes is linked to prelabor biology rather than a reflection of the biology relevant for the maintenance of pregnancy. A piecewise fused LASSO regression analysis was used to provide an estimate as to when before the day of labor such a transition occurs (Fig. 5A). This approach (see Materials and Methods) combined the predictions rho (ρ) of two LASSO regression models built using the data points

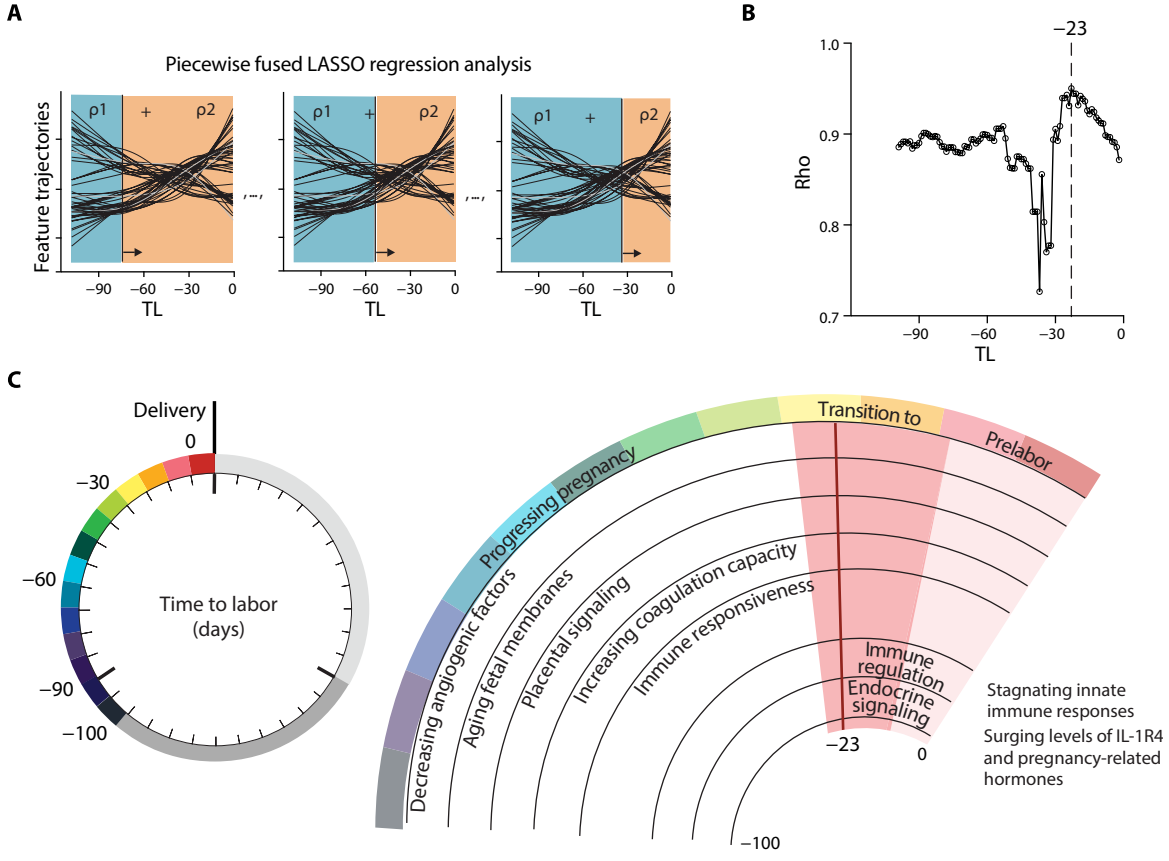


**Fig. 5. A breakpoint in omic trajectories demarcates the transition from pregnancy maintenance to prelabor biological adaptations.** (**A**) Schematic of a piecewise fused LASSO regression combining predictions rho (ρ) of two regression models built from all datasets before and after a particular TL threshold, while sliding the threshold across the time axis. Plotting ρ over time reveals the time point of highest accuracy (maximum ρ). (**B**) Maximum ρ of 0.95 was observed at day −23 (range [−27, −13]; $N = 53$ patients). (**C**) Summary of concerted biological adaptations depicting a clock to labor. Angiogenic factors: Decreased Angiopoietin-2, sTie-2, and VEGF121. Aging fetal membranes: Increased PLXB2 and DDR1. Placental signaling: Increased Activin-A and Siglec-6. Coagulation capacity: Decreased ATIII and increased uPA. Immune responsiveness: Increased Cystatin C, increased pSTAT1 responses in NK and pDC upon IFN-α stimulation, and decreased granulocyte frequencies. A switch to prelabor biology occurs at day −23 (range [−27, −13]; pink shaded phase) before the day of labor. The prelabor phase is characterized by immune regulation: Stagnating pSTAT1 responses in NK and pDC upon IFN-α stimulation, decreased basal IκB and pMK2 signals in $CD4^{+}$ and $CD8^{+}$ T cells, decreased pCREB in ncMC upon GM-CSF stimulation, decreased pSTAT6 responses in DC upon IFN-α stimulation, decreased pMK2 in B cells upon LPS stimulation, and decreased MyD88 responses in cMC upon LPS and GM-CSF stimulation. Regulation of Macrophage inhibitory cytokine-1 (MIC-1), Secretory Leukocyte Peptidase Inhibitor (SLPI), and Lymphocyte-activation gene 3 (LAG3). Surging Cystatin C and IL-1R4. Endocrine signaling: Surging 17-OHP isomers, 17-hydroxypregnenolone sulfate, and cortisol isomer.

before or after a given TL threshold, while varying the threshold across all time points. A maximum ρ value was reached when the models on each side of the threshold contained distinct yet top informative biological features that, when combined, reached maximal predictive accuracy. The piecewise fused LASSO regression analysis produced a maximum at 23 days before the day of labor (range [−27, −13] days; ρ at −23 days = 0.95; Fig. 5B).

Our results indicate that the maternal metabolome, proteome, and immunome undergo a marked transition from maintenance of pregnancy to a phase of prelabor biology that is linked to the timing of labor (Fig. 5C). The model in Fig. 5C summarizes major characteristics of the biology before and after the transition period occurring 2 to 4 weeks before labor.

## DISCUSSION

This study combined the high-content assessment of circulating plasma factors with single-cell analyses of peripheral immune cells to survey dynamic changes in the maternal metabolome, proteome, and immunome preceding the day of labor. Using a stringent analytical method that accounts for the dimensionality and heterogeneity of the data, we built and independently validated a multiomic model that predicted the timing of spontaneous labor.

Current efforts to monitor biological adaptations during pregnancy have primarily been focused on investigating dynamics that differentiate normal from pathological pregnancies on the basis of GA (*12*, *13*, *47*–*53*). Although they are informative in characterizing pathological deviations during pregnancy, these approaches provide limited information for the prediction of timing of labor because they rely on estimates of GA, which are imposed by human assumption rather than based on biological determination. In contrast, our study paradigm did not use an estimate but an observed outcome, such as the time to spontaneous labor. This outcome was independent of GA on the basis of EDD and accounted for the inherent variations in pregnancy duration. Hence, our approach enabled characterization of labor-relevant pathways, which may be important for the identification of labor-specific mechanisms in normal and pathological pregnancies.

In our study, the analysis of metabolic, proteomic, and immunologic trajectories provided an integrated view of response mechanisms associated with the TL. Two major themes evolved: (i) The coordinated adaptations across biological systems revealed a prelabor interactome that pointed toward cross-talk between circulating plasma factors and immune cell responses toward the end of pregnancy, and (ii) dynamics in omic trajectories uncovered a marked transition from pregnancy maintenance to prelabor biology 2 to 4 weeks before delivery.

Aspects of our analysis agree with prior studies of endocrine and inflammatory changes during late pregnancy. For example, steroid hormone metabolites were among the most informative metabolic features of the predictive model, which is consistent with the established role of progesterone in the maintenance of mammalian pregnancy (*54*) and the progression to labor (*20*, *54*, *55*). Similarly, key immune response features of our predictive model are consistent with previous studies reporting on peripheral immune activation with approaching labor (*12*, *17*, *56*–*63*). Specifically, the pSTAT1 signaling in $CD56^{dim}CD16^{+}$ NK cells in response to IFN-α was a key immune feature common to our current model predicting the TL and our previous model predicting GA (*12*). In contrast, the endogenous STAT5 signaling activity in T cells, important for predicting GA (*12*), did not contribute to the current model (fig. S6). Differences in immune features between the two models likely reflect the dynamic evolution of immune signatures throughout pregnancy and underpin that the selection of predictive parameters depends on the window of observation.

Our results also suggest previously undescribed cross-talk between metabolic, proteomic, and immune cell features that precedes the onset of labor. We found that the surge in steroid hormone metabolites 2 to 4 weeks before labor coincided with dynamic changes in plasma protein concentrations and immune cell responses that reflected a previously unrecognized switch from immune activation to regulation of inflammatory responses. One of the most pronounced examples of immune regulation was the surge in the concentration of IL-1R4, which paralleled the dampening of JAK-STAT and MyD88 responses in innate immune cells (Fig. 4, F and J). The data suggest that IL-1R4, an IL-33 antagonist, may play a prominent regulatory role during the prelabor phase by neutralizing IL-33 (*64*), a proinflammatory yet regulatory T cell–stabilizing alarmin released upon tissue remodeling (*42*). In mice, IL-33 has been assigned a pregnancy-maintaining role (*43*). Rising concentrations of IL-1R4 in response to increased IL-33 activity could function as a labor-initiating signal by disrupting IL-33–mediated mechanisms of fetomaternal tolerance (*11*, *19*), while simultaneously counteracting systemic proinflammatory innate responses to accumulating circulating fetal material with approaching parturition (*13*, *65*–*68*).

The observed dampening of systemic inflammatory events with approaching labor contrasts with prior studies showing increased local inflammation of the cervix, decidua, fetal membranes, and placenta during labor and parturition (*46*, *69*, *70*), although several other studies of systemic immune responses during pregnancy echo our findings of decreased peripheral immune cell responses with approaching labor (*47*, *56*, *57*, *60*, *71*, *72*). Hence, the systemic dampening of proinflammatory responses may be important to keep in check proinflammatory events initiated locally with labor onset.

Our multiomic analysis also provided a high-resolution fingerprint of essential biological processes preceding the day of labor, including changes in vascular development, placental biology, and fetal membrane activation (*22*, *73*). Angiogenic factors, potentially involved in placental vascularization, progressively diminished (*35*, *36*, *45*); whereas, coagulation capacity became enhanced (*16*, *17*, *44*). In accordance with previous studies (*16*, *25*, *74*, *75*), placental factors Activin-A and Siglec-6 followed accelerated trajectories, potentially reflecting placental aging (*32*). Increased concentrations of serum Activin-A and placental Siglec-6 are also detected in labor versus nonlabor deliveries (*76*–*78*). In addition, the steady increase of epithelial factors PLXB2 and DDR1 likely mirrors the remodeling of the fetal membranes (*22*). Several of these circulating proteins, including Angiopoietin-2, urokinase-type plasminogen activator (uPA), Activin-A, Siglec-6, PLXB2, and DDR1, have proven to be informative model components for the prediction of GA, both by our group (*79*) and others (*16*, *17*).

The pathway enrichment analysis of the most informative model features provided further insight on previously undescribed biological pathways implicated in the transition from progressing pregnancy to labor onset. First, glycoproteins and proteins associated with glycoprotein metabolism, including ATIII, VEGF121, matrix metalloproteinase 12 (MMP12), Angiopoietin-2, sTie-2, and SLIT and

NTRK-like protein 5 (SLITRK5), were enriched among the proteomic features. SLITRK5 has a high affinity for pregnancy-specific glycoprotein (*80*), an immune tolerance–enhancing protein released from the placenta and peaking in late gestation (*81*). Second, metabolic pathways, including tryptophan metabolism, and pentose/glucuronate interconversions (carbohydrate metabolism) were also enriched. The systemic concentration of serotonin-precursor 5-hydroxytryptophan is a proxy for serotonin activity in the central nervous system and facilitates vasoconstriction in the placenta (*82*, *83*). The involvements of glycoproteins, vasoactive neurotransmitters, and energy metabolism highlight prelabor dynamics beyond previously described fetal and immunoendocrine mechanisms.

Our study has certain limitations. First, the cohort included a homogeneous population of women recruited at a single center, who went into labor predominantly at term ($N = 63$; of which five preterm < 37 weeks, zero postterm > 42 weeks). Hence, our model predicted the TL in term and preterm pregnancies with similar accuracy. Future studies in a more diverse population and enriched for women with extreme pregnancy lengths will be needed to further test the generalizability of our findings. Studies specifically focusing on women with preterm labor will be particularly important because the ability to predict labor several weeks before the actual day of labor provides a critical time window that would aid in clinical decision-making for the early management of a patient at risk of preterm labor. In such studies, it will also be important to refine the predictive models to allow differentiating between labor onset that results in arrested preterm labor versus resulting in a preterm delivery, which our current model cannot resolve. Further, future studies will be required to determine the effect of pregnancy complications such as preeclampsia, chorioamnionitis, or infection on the predictive model parameters reported here. Second, we limited the blood sampling frequency to three samples per patient. Nonetheless, our approach provided highly informative results regarding multiomic adaptations relevant to the TL, which will dovetail with other studies, generating less data with higher per-patient sampling resolution (*84*). Third, our study lacks the assessment of local immune responses. It will be informative to determine the relationship between systemic and local features occurring before and during labor. Last, interactions between features identified within and between datasets remain associations until supported by direct mechanistic evidence. However, on the basis of prior biological knowledge, particular associations between proteins or metabolites and immune cell responses can be hypothesized to be biological interactions.

In summary, determining the timing of labor and delivery, and predicting preterm and postterm pregnancy risk, remains an important clinical challenge. The biological insights of this study may guide therapeutic approaches to extend pregnancy when the labor signature is detected early (preterm birth) or to accelerate labor processes to avoid the need for induction of labor in postdate pregnancies. The results lay the foundation to examine prelabor biology for the development of a universal diagnostic tool that can predict the TL.

## MATERIALS AND METHODS

### Study design

The aim of this observational study was to determine a precise chronology of pregnancy-related metabolomic, proteomic, and immunologic adaptations in venous blood samples collected serially during the last 100 days of pregnancy. The study was conducted at the Lucile Packard Children's Hospital (Stanford, CA, USA) and approved by the Institutional Review Board (approval ID, 40105). All participants signed an informed consent. Healthy pregnant women receiving routine antepartum care were eligible for the study if they were within 18 to 50 years of age, had a BMI < 40 in their second or third trimester of pregnancy as determined by their clinician using LMP and ultrasound estimates of GA, and had no immune-modifying comorbidities or medication usage. Participants were followed longitudinally until parturition, collecting one to three blood samples throughout the third trimester. In total, 112 women were recruited to meet the predetermined sample size required for sufficient power in this longitudinal study. Participants for whom labor was medically induced ($N = 43$) or who underwent cesarean section without labor ($N = 4$) were excluded. Two participants dropped out of the study. Participants with singleton pregnancies, who went into spontaneous labor ($N = 53$ training cohort, $N = 5$ test cohort) or experienced spontaneous rupture of membranes before labor onset ($N = 5$ test cohort) were included in the analysis. The day of labor was defined as day of admission for spontaneous labor (contractions occurring at least every 5 min, lasting >1 min, and associated with cervical change). For five patients from the test cohort, the day of spontaneous rupture of membrane was designated as the day of labor because labor would have likely ensued spontaneously (*85*), but modern clinical care required induction of labor for these patients. The GA at day of sampling was based on the clinical EDD established by LMP and/or ultrasonographic assessment according to the American College of Obstetricians and Gynecologists committee opinion (*8*). Researchers conducting the analyses were not blinded. Randomization was not applicable to this study. Demographics, pregnancy characteristics, and comorbidities for the 63 participants included in the analysis are summarized in Table 1.

### Mass cytometry from whole blood

#### *Ex vivo immunoassay*

Whole blood was collected from study subjects and processed within 60 min after blood draw. Individual aliquots were stimulated for 15 min at 37°C with LPS (1 μg/ml; InvivoGen, San Diego, CA), IFN-α (100 ng/ml; PBL Assay Science, Piscataway, NJ), GM-CSF (100 ng/ml; R&D Systems, Minneapolis, MN), and a cocktail of IL-2, IL-4, and IL-6 (each 100 ng/ml; R&D Systems) or left unstimulated. Samples were processed using a standardized protocol for fixing with proteomic stabilizer (SMART TUBE Inc., San Carlos, CA) and stored at −80°C until further processing.

#### *Mass cytometry and derivation of cell frequency, basal intracellular signaling, and intracellular signaling response features*

Forty-one innate and adaptive immune cell subsets were identified using a 45-parameter mass cytometry antibody panel and according to the gating strategy in fig. S7. Cell frequencies were expressed as a percentage derived from singlet live mononuclear cells ($DNA^+cPARP^-CD235^-CD61^-CD66^-$) except for granulocyte frequencies, which were expressed as a percentage of singlet live leukocytes ($DNA^+cPARP^-CD235^-CD61^-$). Endogenous intracellular signaling activities at the basal, unstimulated state were quantified per single cell for pSTAT1, pSTAT3, pSTAT5, pSTAT6, pCREB, pMK2, pERK, phosphorylated S6 ribosomal protein (prpS6), pP38, and phosphorylated nuclear factor κB (pNF-κB), and total inhibitor of NF-κB (IκB) using an arcsinh-transformed value calculated from the median signal

intensity. Intracellular signaling responses to stimulation were reported as the difference in arcsinh-transformed value of each signaling protein between the stimulated and unstimulated conditions (arcsinh ratio over endogenous signal). A knowledge-based penalization matrix was applied to intracellular signaling response features in the mass cytometry data based on mechanistic immunological knowledge, as previously described (*14*, *86*). Mechanistic priors used in the penalization matrix are independent of immunological knowledge related to pregnancy or the day of labor.

### Proteomics and untargeted metabolomics from plasma

Derivation of proteomic (SomaLogic Inc., Boulder, CO) and metabolomic (liquid chromatography–mass spectrometry) features from plasma samples is described in the Supplementary Materials.

### Statistical analyses

#### *Multivariate modeling and SG*

For a matrix $\mathbf{X}$ of all biological features from a given omic dataset, and a vector of days to day of labor $\mathbf{Y}$, the LASSO algorithm calculates coefficients $\beta$ to minimize the error term $L(\beta) = ||\mathbf{Y} - \mathbf{X}\beta||2$. An $L1$ regularization was used to increase model sparsity for the sake of biological interpretation and model validation. Once a LASSO model was trained for each omics modality, the multiomic analysis was carried out by performing SG on the new representation of the data by using the outputs of the previous layer of models as predictors. A LASSO model was first constructed on each omic modality. Then, all estimations of TL were used as predictors for a second-layer LASSO model. Intrinsically, this is equivalent to a weighted average of the individual models with the coefficients of the LASSO model as desired weights. A two-layer leave-one-subject-out cross-validation strategy was used to assess the generalizability of the SG model built on the training cohort (see the Supplementary Materials). Performance for training and validation was evaluated using RMSE, and the test statistic is based on Pearson's product moment correlation coefficient. The asymptotic confidence interval is given on the basis of Fisher's $Z$ transform.

#### *Piecewise fused LASSO regression*

To identify a possible "switch point" before labor, we used two sequential LASSO models applied to all samples before/after a given threshold. Cross-validation predictions from both models were combined to develop a joint goodness-of-fit score for the entire dataset. The threshold was varied across the dataset to identify the point with the best fit for the combined models. Fused LASSO (*87*, *88*), a generalized LASSO for one-dimensional sequential data, which penalizes the absolute differences in successive coordinates of the LASSO coefficients, was used to detect the interval in which the joint models had the strongest predictive power, representing the region where the maximal change of biological behavior occurs before delivery.

## SUPPLEMENTARY MATERIALS

stm.sciencemag.org/cgi/content/full/13/592/eabd9898/DC1
Materials and Methods
Fig. S1. Analyses of the subcohort of patients with preterm (PT) labor.
Fig. S2. Metabolic features most informative for the integrated prediction model ($N = 53$ patients, $n = 150$ samples, training cohort).
Fig. S3. Proteomic features most informative for the integrated prediction model ($N = 53$ patients, $n = 150$ samples, training cohort).
Fig. S4. Immune features most informative for the integrated prediction model ($N = 53$ patients, $n = 150$ samples, training cohort).
Fig. S5. Innate immune responsiveness decelerates in the prelabor phase ($N = 53$ patients, $n = 150$ samples, training cohort).
Fig. S6. Basal adaptive immune activity in the prelabor phase ($N = 53$ patients, $n = 150$ samples, training cohort).
Fig. S7. Gating strategy for mass cytometry analyses.
Table S1. Mass cytometry antibody panel.
Table S2. Confounder analysis.
Table S3. Forty-five most informative features of the integrated multiomic labor prediction model in the training (blue) and test (gray) cohort.
Table S4. Goodness of fit of a pattern-fitting model [Akaike information criterion (AIC)] for the 45 most informative features of the integrated multiomic labor prediction model in the training cohort.
References (*89*–*91*)

View/request a protocol for this paper from *Bio-protocol*.

## REFERENCES AND NOTES


1. L. Liu, S. Oza, D. Hogan, Y. Chu, J. Perin, J. Zhu, J. E. Lawn, S. Cousens, C. Mathers, R. E. Black, Global, regional, and national causes of under-5 mortality in 2000-15: An updated systematic analysis with implications for the Sustainable Development Goals. *Lancet* **388**, 3027–3035 (2016).
2. M. Galal, I. Symonds, H. Murray, F. Petraglia, R. Smith, Postterm pregnancy. *Facts Views Vis. Obgyn.* **4**, 175–187 (2012).
3. H. M. Georgiou, M. K. W. Di Quinzio, M. Permezel, S. P. Brennecke, Predicting preterm labour: Current status and future prospects. *Dis. Markers* **2015**, 435014 (2015).
4. N. Suff, L. Story, A. Shennan, The prediction of preterm delivery: What is new? *Semin. Fetal Neonatal Med.* **24**, 27–32 (2019).
5. J. Hutcheon, L. Lee, G. Marquette, 320: Predicting the onset of spontaneous labour (OSL) in post date pregnancies. *Am. J. Obstet. Gynecol.* **208**, S143–S144 (2013).
6. W. B. Barr, C. C. Pecci, Last menstrual period versus ultrasound for pregnancy dating. *Int. J. Gynaecol. Obstet.* **87**, 38–39 (2004).
7. D. A. Savitz, J. W. Terry Jr., N. Dole, J. M. Thorp Jr., A. M. Siega-Riz, A. H. Herring, Comparison of pregnancy dating by last menstrual period, ultrasound scanning, and their combination. *Am. J. Obstet. Gynecol.* **187**, 1660–1666 (2002).
8. Committee on Obstetric Practice American Institute of Ultrasound in Medicine Society for Maternal–Fetal Medicine, Committee Opinion No 700: Methods for estimating the due date. *Obstet. Gynecol.* **129**, e150–e154 (2017).
9. L. S. Peterson, I. A. Stelzer, A. S. Tsai, M. S. Ghaemi, X. Han, K. Ando, V. D. Winn, N. R. Martinez, K. Contrepois, M. N. Moufarrej, S. Quake, D. A. Relman, M. P. Snyder, G. M. Shaw, D. K. Stevenson, R. J. Wong, P. Arck, M. S. Angst, N. Aghaeepour, B. Gaudilliere, Multiomic immune clockworks of pregnancy. *Semin. Immunopathol.* **42**, 397–412 (2020).
10. M. PrabhuDas, E. Bonney, K. Caron, S. Dey, A. Erlebacher, A. Fazleabas, S. Fisher, T. Golos, M. Matzuk, J. M. McCune, G. Mor, L. Schulz, M. Soares, T. Spencer, J. Strominger, S. S. Way, K. Yoshinaga, Immune mechanisms at the maternal-fetal interface: Perspectives and challenges. *Nat. Immunol.* **16**, 328–334 (2015).
11. P. C. Arck, K. Hecher, Fetomaternal immune cross-talk and its consequences for maternal and offspring's health. *Nat. Med.* **19**, 548–556 (2013).
12. N. Aghaeepour, E. A. Ganio, D. McIlwain, A. S. Tsai, M. Tingle, S. Van Gassen, D. K. Gaudilliere, Q. Baca, L. McNeil, R. Okada, M. S. Ghaemi, D. Furman, R. J. Wong, V. D. Winn, M. L. Druzin, Y. Y. El-Sayed, C. Quaintance, R. Gibbs, G. L. Darmstadt, G. M. Shaw, D. K. Stevenson, R. Tibshirani, G. P. Nolan, D. B. Lewis, M. S. Angst, B. Gaudilliere, An immune clock of human pregnancy. *Sci. Immunol.* **2**, eaan2946 (2017).
13. T. T. M. Ngo, M. N. Moufarrej, M.-L. H. Rasmussen, J. Camunas-Soler, W. Pan, J. Okamoto, N. F. Neff, K. Liu, R. J. Wong, K. Downes, R. Tibshirani, G. M. Shaw, L. Skotte, D. K. Stevenson, J. R. Biggio, M. A. Elovitz, M. Melbye, S. R. Quake, Noninvasive blood tests for fetal development predict gestational age and preterm delivery. *Science* **360**, 1133–1136 (2018).
14. M. S. Ghaemi, D. B. DiGiulio, K. Contrepois, B. Callahan, T. T. M. Ngo, B. Lee-McMullen, B. Lehallier, A. Robaczewska, D. Mcilwain, Y. Rosenberg-Hasson, R. J. Wong, C. Quaintance, A. Culos, N. Stanley, A. Tanada, A. Tsai, D. Gaudilliere, E. Ganio, X. Han, K. Ando, L. McNeil, M. Tingle, P. Wise, I. Maric, M. Sirota, T. Wyss-Coray, V. D. Winn, M. L. Druzin, R. Gibbs, G. L. Darmstadt, D. B. Lewis, V. P. Nia, B. Agard, R. Tibshirani, G. Nolan, M. P. Snyder, D. A. Relman, S. R. Quake, G. M. Shaw, D. K. Stevenson, M. S. Angst, B. Gaudilliere, N. Aghaeepour, Multiomics modeling of the immunome, transcriptome, microbiome, proteome and metabolome adaptations during human pregnancy. *Bioinformatics* **35**, 95–103 (2019).
15. N. Gomez-Lopez, R. Romero, S. S. Hassan, G. Bhatti, S. M. Berry, J. P. Kusanovic, P. Pacora, A. L. Tarca, The cellular transcriptome in the maternal circulation during normal pregnancy: A longitudinal study. *Front. Immunol.* **10**, 2863 (2019).

16. R. Romero, O. Erez, E. Maymon, P. Chaemsaithong, Z. Xu, P. Pacora, T. Chaiworapongsa, B. Done, S. S. Hassan, A. L. Tarca, The maternal plasma proteome changes as a function of gestational age in normal pregnancy: A longitudinal study. *Am. J. Obstet. Gynecol.* **217**, 67.e1–67.e21 (2017).
17. R. Apps, Y. Kotliarov, F. Cheung, K. L. Han, J. Chen, A. Biancotto, A. Babyak, H. Zhou, R. Shi, L. Barnhart, S. M. Osgood, Y. Belkaid, S. M. Holland, J. S. Tsang, C. S. Zerbe, Multimodal immune phenotyping of maternal peripheral blood in normal human pregnancy. *JCI Insight* **5**, e134838 (2020).
18. O. Shynlova, Y.-H. Lee, K. Srikhajon, S. J. Lye, Physiologic uterine inflammation and labor onset: Integration of endocrine and mechanical signals. *Reprod. Sci.* **20**, 154–167 (2013).
19. N. Gomez-Lopez, D. StLouis, M. A. Lehr, E. N. Sanchez-Rodriguez, M. Arenas-Hernandez, Immune cells in term and preterm labor. *Cell. Mol. Immunol.* **11**, 571–581 (2014).
20. C. R. Mendelson, Minireview: Fetal-maternal hormonal signaling in pregnancy and labor. *Mol. Endocrinol.* **23**, 947–954 (2009).
21. M. McLean, A. Bisits, J. Davies, R. Woods, P. Lowry, R. Smith, A placental clock controlling the length of human pregnancy. *Nat. Med.* **1**, 460–463 (1995).
22. R. Menon, L. S. Richardson, M. Lappas, Fetal membrane architecture, aging and inflammation in pregnancy and parturition. *Placenta* **79**, 40–45 (2019).
23. E. R. Norwitz, J. N. Robinson, J. R. Challis, The control of labor. *N. Engl. J. Med.* **341**, 660–666 (1999).
24. F. G. Cunningham, K. J. Leveno, S. L. Bloom, C. Y. Spong, J. S. Dashe, B. L. Hoffman, B. M. Casey, J. S. Sheffield, *Williams Obstetrics* (McGraw Hill, ed. 24, 2013); http://accessmedicine.mhmedical.com/content.aspx?bookid=1057&sectionid=59789161.
25. A. L. Tarca, R. Romero, N. Benshalom-Tirosh, N. G. Than, D. W. Gudicha, B. Done, P. Pacora, T. Chaiworapongsa, B. Panaitescu, D. Tirosh, N. Gomez-Lopez, S. Draghici, S. S. Hassan, O. Erez, The prediction of early preeclampsia: Results from a longitudinal proteomics study. *PLOS ONE* **14**, e0217273 (2019).
26. K. Contrepois, L. Jiang, M. Snyder, Optimized analytical procedures for the untargeted metabolomic profiling of human urine and plasma by combining hydrophilic interaction (HILIC) and reverse-phase liquid chromatography (RPLC)-mass spectrometry. *Mol. Cell. Proteomics* **14**, 1684–1695 (2015).
27. L. Gold, D. Ayers, J. Bertino, C. Bock, A. Bock, E. N. Brody, J. Carter, A. B. Dalby, B. E. Eaton, T. Fitzwater, D. Flather, A. Forbes, T. Foreman, C. Fowler, B. Gawande, M. Goss, M. Gunn, S. Gupta, D. Halladay, J. Heil, J. Heilig, B. Hicke, G. Husar, N. Janjic, T. Jarvis, S. Jennings, E. Katilius, T. R. Keeney, N. Kim, T. H. Koch, S. Kraemer, L. Kroiss, N. Le, D. Levine, W. Lindsey, B. Lollo, W. Mayfield, M. Mehan, R. Mehler, S. K. Nelson, M. Nelson, D. Nieuwlandt, M. Nikrad, U. Ochsner, R. M. Ostroff, M. Otis, T. Parker, S. Pietrasiewicz, D. I. Resnicow, J. Rohloff, G. Sanders, S. Sattin, D. Schneider, B. Singer, M. Stanton, A. Sterkel, A. Stewart, S. Stratford, J. D. Vaught, M. Vrkljan, J. J. Walker, M. Watrobka, S. Waugh, A. Weiss, S. K. Wilcox, A. Wolfson, S. K. Wolk, C. Zhang, D. Zichi, Aptamer-based multiplexed proteomic technology for biomarker discovery. *PLOS ONE* **5**, e15004 (2010).
28. D. H. Wolpert, Stacked generalization. *Neural Netw.* **5**, 241–259 (1992).
29. I. Rivals, L. Personnaz, L. Taing, M.-C. Potier, Enrichment or depletion of a GO category within a class of genes: Which test? *Bioinformatics* **23**, 401–407 (2007).
30. J. Xia, I. V. Sinelnikov, B. Han, D. S. Wishart, MetaboAnalyst 3.0—Making metabolomics more meaningful. *Nucleic Acids Res.* **43**, W251–W257 (2015).
31. B. R. Carr, C. R. Parker Jr., J. D. Madden, P. C. MacDonald, J. C. Porter, Maternal plasma adrenocorticotropin and cortisol relationships throughout human pregnancy. *Am. J. Obstet. Gynecol.* **139**, 416–422 (1981).
32. R. Tai, H. S. Taylor, *Endocrinology of Pregnancy* (MDText.com Inc., 2000); https://www.ncbi.nlm.nih.gov/books/NBK278962/.
33. H. Singh, J. D. Aplin, Endometrial apical glycoproteomic analysis reveals roles for cadherin 6, desmoglein-2 and plexin b2 in epithelial integrity. *Mol. Hum. Reprod.* **21**, 81–94 (2015).
34. W. F. Vogel, A. Aszódi, F. Alves, T. Pawson, Discoidin domain receptor 1 tyrosine kinase has an essential role in mammary gland development. *Mol. Cell. Biol.* **21**, 2906–2917 (2001).
35. E. Geva, D. G. Ginzinger, C. J. Zaloudek, D. H. Moore, A. Byrne, R. B. Jaffe, Human placental vascular development: Vasculogenic and angiogenic (branching and nonbranching) transformation is regulated by vascular endothelial growth factor-A, angiopoietin-1, and angiopoietin-2. *J. Clin. Endocrinol. Metab.* **87**, 4213–4224 (2002).
36. M. Bolin, E. Wiberg-Itzel, A.-K. Wikström, M. Goop, A. Larsson, M. Olovsson, H. Akerud, Angiopoietin-1/angiopoietin-2 ratio for prediction of preeclampsia. *Am. J. Hypertens.* **22**, 891–895 (2009).
37. D. Tulchinsky, H. H. Simmer, Sources of plasma 17$\alpha$-hydroxyprogesterone in human pregnancy. *J. Clin. Endocrinol. Metab.* **35**, 799–808 (1972).
38. M. Abbassi-Ghanavati, L. G. Greer, F. G. Cunningham, Pregnancy and laboratory studies: A reference table for clinicians. *Obstet. Gynecol.* **114**, 1326–1331 (2009).
39. K. D. Pennell, M. A. Woodin, P. B. Pennell, Quantification of neurosteroids during pregnancy using selective ion monitoring mass spectrometry. *Steroids* **95**, 24–31 (2015).
40. I. Granne, J. H. Southcombe, J. V. Snider, D. S. Tannetta, T. Child, C. W. G. Redman, I. L. Sargent, ST2 and IL-33 in pregnancy and pre-eclampsia. *PLOS ONE* **6**, e24463 (2011).
41. R. Romero, P. Chaemsaithong, A. L. Tarca, S. J. Korzeniewski, E. Maymon, P. Pacora, B. Panaitescu, N. Chaiyasit, Z. Dong, O. Erez, S. S. Hassan, T. Chaiworapongsa, Maternal plasma-soluble ST2 concentrations are elevated prior to the development of early and late onset preeclampsia - a longitudinal study. *J. Matern. Fetal Neonatal Med.* **31**, 418–432 (2018).
42. F. Y. Liew, J.-P. Girard, H. R. Turnquist, Interleukin-33 in health and disease. *Nat. Rev. Immunol.* **16**, 676–689 (2016).
43. B. Huang, A. N. Faucette, M. D. Pawlitz, B. Pei, J. W. Goyert, J. Z. Zhou, N. G. El-Hage, J. Deng, J. Lin, F. Yao, R. S. Dewar III, J. S. Jassal, M. L. Sandberg, J. Dai, M. Cols, C. Shen, L. A. Polin, R. A. Nichols, T. B. Jones, M. H. Bluth, K. S. Puder, B. Gonik, N. R. Nayak, E. Puscheck, W. Z. Wei, A. Cerutti, M. Colonna, K. Chen, Interleukin-33-induced expression of PIBF1 by decidual B cells protects against preterm labor. *Nat. Med.* **23**, 128–135 (2017).
44. A. H. James, E. Rhee, B. Thames, C. S. Philipp, Characterization of antithrombin levels in pregnancy. *Thromb. Res.* **134**, 648–651 (2014).
45. C. S. Buhimschi, V. Bhandari, A. T. Dulay, S. Thung, S. S. Abdel- Razeq, V. Rosenberg, C. S. Han, U. A. Ali, E. Zambrano, G. Zhao, E. F. Funai, I. A. Buhimschi, Amniotic fluid angiopoietin-1, angiopoietin-2, and soluble receptor tunica interna endothelial cell kinase-2 levels and regulation in normal pregnancy and intraamniotic inflammation-induced preterm birth. *J. Clin. Endocrinol. Metab.* **95**, 3428–3436 (2010).
46. N. Gomez-Lopez, L. Vadillo-Perez, S. Nessim, D. M. Olson, F. Vadillo-Ortega, Choriodecidua and amnion exhibit selective leukocyte chemotaxis during term human labor. *Am. J. Obstet. Gynecol.* **204**, 364.e9–364.e16 (2011).
47. C. Seiler, N. L. Bayless, R. Vergara, J. Pintye, J. Kinuthia, L. Osborn, D. Matemo, B. A. Richardson, G. John-Stewart, S. Holmes, C. A. Blish, Influenza-induced interferon lambda response is associated with longer time to delivery among pregnant Kenyan women. *Front. Immunol.* **11**, 452 (2020).
48. X. Han, M. S. Ghaemi, K. Ando, L. S. Peterson, E. A. Ganio, A. S. Tsai, D. K. Gaudilliere, I. A. Stelzer, J. Einhaus, B. Bertrand, N. Stanley, A. Culos, A. Tanada, J. Hedou, E. S. Tsai, R. Fallahzadeh, R. J. Wong, A. E. Judy, V. D. Winn, M. L. Druzin, Y. J. Blumenfeld, M. A. Hlatky, C. C. Quaintance, R. S. Gibbs, B. Carvalho, G. M. Shaw, D. K. Stevenson, M. S. Angst, N. Aghaeepour, B. Gaudilliere, Differential dynamics of the maternal immune system in healthy pregnancy and preeclampsia. *Front. Immunol.* **10**, 1305 (2019).
49. J. Ghartey, L. Anglim, J. Romero, A. Brown, M. A. Elovitz, Women with symptomatic preterm birth have a distinct cervicovaginal metabolome. *Am. J. Perinatol.* **34**, 1078–1083 (2017).
50. J. M. Fettweis, M. G. Serrano, J. P. Brooks, D. J. Edwards, P. H. Girerd, H. I. Parikh, B. Huang, T. J. Arodz, L. Edupuganti, A. L. Glascock, J. Xu, N. R. Jimenez, S. C. Vivadelli, S. S. Fong, N. U. Sheth, S. Jean, V. Lee, Y. A. Bokhari, A. M. Lara, S. D. Mistry, R. A. Duckworth III, S. P. Bradley, V. N. Koparde, X. V. Orenda, S. H. Milton, S. K. Rozycki, A. V. Matveyev, M. L. Wright, S. V. Huzurbazar, E. M. Jackson, E. Smirnova, J. Korlach, Y.-C. Tsai, M. R. Dickinson, J. L. Brooks, J. I. Drake, D. O. Chaffin, A. L. Sexton, M. G. Gravett, C. E. Rubens, N. R. Wijesooriya, K. D. Hendricks-Muñoz, K. K. Jefferson, J. F. Strauss III, G. A. Buck, The vaginal microbiome and preterm birth. *Nat. Med.* **25**, 1012–1021 (2019).
51. E. Amabebe, D. R. Chapman, V. L. Stern, G. Stafford, D. O. C. Anumba, Mid-gestational changes in cervicovaginal fluid cytokine levels in asymptomatic pregnant women are predictive markers of inflammation-associated spontaneous preterm birth. *J. Reprod. Immunol.* **126**, 1–10 (2018).
52. I. Kosti, S. Lyalina, K. S. Pollard, A. J. Butte, M. Sirota, Meta-analysis of vaginal microbiome data provides new insights into preterm birth. *Front. Microbiol.* **11**, 476 (2020).
53. G. R. Saade, K. A. Boggess, S. A. Sullivan, G. R. Markenson, J. D. Iams, D. V. Coonrod, L. M. Pereira, M. S. Esplin, L. M. Cousins, G. K. Lam, M. K. Hoffman, R. D. Severinsen, T. Pugmire, J. S. Flick, A. C. Fox, A. J. Lueth, S. R. Rust, E. Mazzola, C. Hsu, M. T. Dufford, C. L. Bradford, I. E. Ichetovkin, T. C. Fleischer, A. D. Polpitiya, G. C. Critchfield, P. E. Kearney, J. J. Boniface, D. E. Hickok, Development and validation of a spontaneous preterm delivery predictor in asymptomatic women. *Am. J. Obstet. Gynecol.* **214**, 633.e1–633.e24 (2016).
54. N. M. Shah, P. F. Lai, N. Imami, M. R. Johnson, Progesterone-related immune modulation of pregnancy and labor. *Front. Endocrinol. (Lausanne)* **10**, 198 (2019).
55. S. Mesiano, Myometrial progesterone responsiveness. *Semin. Reprod. Med.* **25**, 005–013 (2007).
56. N. M. Shah, A. A. Herasimtschuk, A. Boasso, A. Benlahrech, D. Fuchs, N. Imami, M. R. Johnson, Changes in T cell and dendritic cell phenotype from mid to late pregnancy are indicative of a shift from immune tolerance to immune activation. *Front. Immunol.* **8**, 1138 (2017).

57. P. Luppi, C. Haluszczak, D. Betters, C. A. H. Richard, M. Trucco, J. A. DeLoia, Monocytes are progressively activated in the circulation of pregnant women. *J. Leukoc. Biol.* **72**, 874–884 (2002).
58. K. Taniguchi, H. Nagata, T. Katsuki, C. Nakashima, R. Onodera, A. Hiraoka, N. Takata, M. Kobayashi, M. Kambe, Significance of human neutrophil antigen-2a (NB1) expression and neutrophil number in pregnancy. *Transfusion* **44**, 581–585 (2004).
59. S. Lurie, E. Rahamim, I. Piper, A. Golan, O. Sadan, Total and differential leukocyte counts percentiles in normal pregnancy. *Eur. J. Obstet. Gynecol. Reprod. Biol.* **136**, 16–19 (2008).
60. S. M. Ziegler, C. N. Feldmann, S. H. Hagen, L. Richert, T. Barkhausen, J. Goletzke, V. Jazbutyte, G. Martrus, W. Salzberger, T. Renné, K. Hecher, A. Diemert, P. C. Arck, M. Altfeld, Innate immune responses to toll-like receptor stimulation are altered during the course of pregnancy. *J. Reprod. Immunol.* **128**, 30–37 (2018).
61. A. L. Tarca, R. Romero, Z. Xu, N. Gomez-Lopez, O. Erez, C.-D. Hsu, S. S. Hassan, V. J. Carey, Targeted expression profiling by RNA-Seq improves detection of cellular dynamics during pregnancy and identifies a role for T cells in term parturition. *Sci. Rep.* **9**, 848 (2019).
62. R. Pique-Regi, R. Romero, A. L. Tarca, E. D. Sendler, Y. Xu, V. Garcia-Flores, Y. Leng, F. Luca, S. S. Hassan, N. Gomez-Lopez, Single cell transcriptional signatures of the human placenta in term and preterm parturition. *eLife* **8**, e52004 (2019).
63. R. Obrenovic, D. Petrovic, N. Majkic-Singh, J. Trbojevic-Stankovic, B. Stojimirovic, Serum cystatin C levels in normal pregnancy. *Clin. Nephrol.* **76**, 174–179 (2011).
64. R. Menon, Initiation of human parturition: Signaling from senescent fetal tissues via extracellular vesicle mediated paracrine mechanism. *Obstet. Gynecol. Sci.* **62**, 199–211 (2019).
65. J. Polettini, F. Behnia, B. D. Taylor, G. R. Saade, R. N. Taylor, R. Menon, Telomere fragment induced amnion cell senescence: A contributor to parturition? *PLOS ONE* **10**, e0137188 (2015).
66. M. D. Mitchell, H. N. Peiris, M. Kobayashi, Y. Q. Koh, G. Duncombe, S. E. Illanes, G. E. Rice, C. Salomon, Placental exosomes in normal and complicated pregnancy. *Am. J. Obstet. Gynecol.* **213**, S173–S181 (2015).
67. Y. M. D. Lo, N. Corbetta, P. F. Chamberlain, V. Rai, I. L. Sargent, C. W. G. Redman, J. S. Wainscoat, Presence of fetal DNA in maternal plasma and serum. *Lancet* **350**, 485–487 (1997).
68. J. M. Kinder, I. A. Stelzer, P. C. Arck, S. S. Way, Immunological implications of pregnancy-induced microchimerism. *Nat. Rev. Immunol.* **17**, 483–494 (2017).
69. R. Menon, F. Behnia, J. Polettini, G. R. Saade, J. Campisi, M. Velarde, Placental membrane aging and HMGB1 signaling associated with human parturition. *Aging (Albany NY)* **8**, 216–230 (2016).
70. F. Gotsch, R. Romero, J. P. Kusanovic, O. Erez, J. Espinoza, C. J. Kim, E. Vaisbuch, N. G. Than, S. Mazaki-Tovi, T. Chaiworapongsa, M. Mazor, B. H. Yoon, S. Edwin, R. Gomez, P. Mittal, S. S. Hassan, S. Sharma, The anti-inflammatory limb of the immune response in preterm labor, intra-amniotic infection/inflammation, and spontaneous parturition at term: A role for interleukin-10. *J. Matern. Fetal Neonatal Med.* **21**, 529–547 (2008).
71. T. A. Kraus, S. M. Engel, R. S. Sperling, L. Kellerman, Y. Lo, S. Wallenstein, M. M. Escribese, J. L. Garrido, T. Singh, M. Loubeau, T. M. Moran, Characterizing the pregnancy immune phenotype: Results of the viral immunity and pregnancy (VIP) study. *J. Clin. Immunol.* **32**, 300–311 (2012).
72. I. P. Crocker, P. N. Baker, J. Fletcher, Neutrophil function in pregnancy and rheumatoid arthritis. *Ann. Rheum. Dis.* **59**, 555–564 (2000).
73. J. M. Cha, D. M. Aronoff, A role for cellular senescence in birth timing. *Cell Cycle* **16**, 2023–2031 (2017).
74. L. Yu, D. Li, Q.-p. Liao, H.-x. Yang, B. Cao, G. Fu, G. Ye, Y. Bai, H. Wang, N. Cui, M. Liu, Y.-x. Li, J. Li, C. Peng, Y.-l. Wang, High levels of activin A detected in preeclamptic placenta induce trophoblast cell apoptosis by promoting nodal signaling. *J. Clin. Endocrinol. Metab.* **97**, E1370–E1379 (2012).
75. S. Muttukrishna, P. A. Fowler, L. George, N. P. Groome, P. G. Knight, Changes in peripheral serum levels of total activin A during the human menstrual cycle and pregnancy. *J. Clin. Endocrinol. Metab.* **81**, 3328–3334 (1996).
76. M. P. Plevyak, G. M. Lambert-Messerlian, A. Farina, N. P. Groome, J. A. Canick, H. M. Silver, Concentrations of serum total activin A and inhibin A in preterm and term labor patients: A cross-sectional study. *J. Soc. Gynecol. Investig.* **10**, 231–236 (2003).
77. K. K. Rumer, J. Uyenishi, M. C. Hoffman, B. M. Fisher, V. D. Winn, Siglec-6 expression is increased in placentas from pregnancies complicated by preterm preeclampsia. *Reprod. Sci.* **20**, 646–653 (2013).
78. E. C. M. Brinkman-Van der Linden, N. Hurtado-Ziola, T. Hayakawa, L. Wiggleton, K. Benirschke, A. Varki, N. Varki, Human-specific expression of Siglec-6 in the placenta. *Glycobiology* **17**, 922–931 (2007).
79. N. Aghaeepour, B. Lehallier, Q. Baca, E. A. Ganio, R. J. Wong, M. S. Ghaemi, A. Culos, Y. Y. El-Sayed, Y. J. Blumenfeld, M. L. Druzin, V. D. Winn, R. S. Gibbs, R. Tibshirani, G. M. Shaw, D. K. Stevenson, B. Gaudilliere, M. S. Angst, A proteomic clock of human pregnancy. *Am. J. Obstet. Gynecol.* **218**, 347.e1–347.e14 (2018).
80. M. E. Sowa, E. J. Bennett, S. P. Gygi, J. W. Harper, Defining the human deubiquitinating enzyme interaction landscape. *Cell* **138**, 389–403 (2009).
81. S. M. Blois, G. Sulkowski, I. Tirado-González, J. Warren, N. Freitag, B. F. Klapp, D. Rifkin, I. Fuss, W. Strober, G. S. Dveksler, Pregnancy-specific glycoprotein 1 (PSG1) activates TGF-β and prevents dextran sodium sulfate (DSS)-induced colitis in mice. *Mucosal Immunol.* **7**, 348–358 (2014).
82. N. Carretti, A. Bertazzo, S. Comai, C. V. L. Costa, G. Allegri, F. Petraglia, Serum tryptophan and 5-hydroxytryptophan at birth and during post-partum days. *Adv. Exp. Med. Biol.* **527**, 757–760 (2003).
83. M. A. Cruz, V. Gallardo, P. Miguel, G. Carrasco, C. González, Serotonin-induced vasoconstriction is mediated by thromboxane release and action in the human fetal-placental circulation. *Placenta* **18**, 197–204 (1997).
84. L. Liang, M.-L. H. Rasmussen, B. Piening, X. Shen, S. Chen, H. Röst, J. K. Snyder, R. Tibshirani, L. Skotte, N. C. Y. Lee, K. Contrepois, B. Feenstra, H. Zackriah, M. Snyder, M. Melbye, Metabolic dynamics and prediction of gestational age and time to delivery in pregnant women. *Cell* **181**, 1680–1692.e15 (2020).
85. B. M. Mercer, E. K. S. Chien, in *Gabbe's Obstetrics: Normal and Problem Pregnancies* (Elsevier, ed. 8, 2021), chap. 37, pp. 694–707.e3.
86. A. Culos, A. S. Tsai, N. Stanley, M. Becker, M. S. Ghaemi, D. R. McIlwain, R. Fallahzadeh, A. Tanada, H. Nassar, C. Espinosa, M. Xenochristou, E. Ganio, L. Peterson, X. Han, I. A. Stelzer, K. Ando, D. Gaudilliere, T. Phongpreecha, I. Marić, A. L. Chang, G. M. Shaw, D. K. Stevenson, S. Bendall, K. L. Davis, W. Fantl, G. P. Nolan, T. Hastie, R. Tibshirani, M. S. Angst, B. Gaudilliere, N. Aghaeepour, Integration of mechanistic immunological knowledge into a machine learning pipeline improves predictions. *Nat. Mach. Intell.* **2**, 619–628 (2020).
87. S. Aminikhanghahi, D. J. Cook, A survey of methods for time series change point detection. *Knowl. Inf. Syst.* **51**, 339–367 (2017).
88. R. Tibshirani, M. Saunders, S. Rosset, J. Zhu, K. Knight, Sparsity and smoothness via the fused lasso. *J. R. Stat. Soc. B* **67**, 91–108 (2005).
89. R. Finck, E. F. Simonds, A. Jager, S. Krishnaswamy, K. Sachs, W. Fantl, D. Pe'er, G. P. Nolan, S. C. Bendall, Normalization of mass cytometry data with bead standards. *Cytometry* **83A**, 483–494 (2013).
90. E. R. Zunder, R. Finck, G. K. Behbehani, E. D. Amir, S. Krishnaswamy, V. D. Gonzalez, C. G. Lorang, Z. Bjornson, M. H. Spitzer, B. Bodenmiller, W. J. Fantl, D. Pe'er, G. P. Nolan, Palladium-based mass tag cell barcoding with a doublet-filtering scheme and single-cell deconvolution algorithm. *Nat. Protoc.* **10**, 316–333 (2015).
91. J. C. Rohloff, A. D. Gelinas, T. C. Jarvis, U. A. Ochsner, D. J. Schneider, L. Gold, N. Janjic, Nucleic acid ligands with protein-like side chains: Modified aptamers and their use as diagnostic and therapeutic agents. *Mol. Ther. Nucleic Acids* **3**, e201 (2014).


**Acknowledgments:** We would like to thank C. C. Quaintance, A. G. Yabut, A. Campos, O. Tigre, and H. Romero from the March of Dimes Prematurity Research Center at the Stanford University for help in patient recruitment and sample processing. **Funding:** The study was supported, in part, by the Doris Duke Charitable Foundation (to B.G.); the Burroughs Wellcome Fund (to N.A.); the German Research Foundation (STE2757/1-1 to I.A.S.); the Stanford Maternal and Child Health Research Institute Grant and Postdoctoral Award (to X.H.); the Prematurity Research Fund; the March of Dimes Prematurity Research Center at Stanford University (no. 22FY19343); the Bill and Melinda Gates Foundation (OPP1189911) and the Center for Human Systems Immunology pilot seed grant (to B.G., N.A., M.S.A., and D.K.S.); the Charles B. and Ann L. Johnson Research Fund, the Christopher Hess Research Fund, the Providence Foundation Research Fund, the Roberts Foundation Research Fund, and the Stanford Maternal and Child Health Research Institute (to D.K.S., R.J.W., B.G., N.A., and M.S.A.); the Charles and Mary Robertson Foundation (to B.G., N.A., and D.K.S.); the National Institute of Health [R01AG058417, R01HL13984401, R21DE02772801, and R61NS114926 (to B.G., M.S.A., and N.A.); R01HL13984403 (to V.D.W., B.G., and N.A.); 2RM1HG00773506 (to M.P.S.); R35GM138353 (to N.A.); and R35GM137936 (to B.G.)]; the American Heart Association (18IPA34170507 to M.S.A.); and the Stanford Maternal Child and Health Research Institute Harmon Faculty Scholar Award, H&H Evergreen Faculty Scholar Award (to V.D.W.), and the Stanford Metabolic Health Center (to M.P.S. and K.C.). **Author contributions**: Conceptualization: B.G., N.A., M.S.A., I.A.S., X.H., and V.D.W. Data curation: K.C., M.S.G., B.G., N.A., and M.S.A. Formal analysis: M.S.G., I.A.S., X.H., and J.H. Funding acquisition: M.P.S., B.G., N.A., and M.S.A. Investigation/data acquisition: K.A., X.H., E.A.G., I.A.S., D.F., L.P., K.K.R., E.S.T., D.K.G., A.S.T., B. Choisy, L.P.G., F.V., D.J., S.G., G.M.T., and M.E. Methodology: K.C., B.G., M.S.G., and N.A. Project administration: B.G. and D.K.S. Resources: K.A., B.C., and V.D.W. Software: M.S.G., N.A., J.H., N.S., M.B., A.C., and R.F. Supervision: B.G., N.A., M.S.A., K.C., M.P.S., R.J.W., G.L.D., M.L.D., V.D.W., R.S.G., X.B.L., K.S., B. Carvalho, G.M.S., and D.K.S. Visualization: I.A.S., M.S.G., X.H., and J.H. Writing (original draft): B.G., I.A.S., and X.H. Writing (review and editing): B.G., N.A.,

M.S.A., I.A.S., X.H., D.F., R.J.W., K.C., V.D.W., and all authors. **Competing interests:** A provisional patent application that covers aspects of the subject matter of the paper has been filed (US 63/066,708; title: Compositions and methods of predicting time to onset of labor; coinventors: B.G., N.A., M.S.A., I.A.S., S.G., X.H., K.A., and J.H.). M.P.S. is a founder and member of the science advisory board of Personalis, SensOmics, Qbio, January, Mirvie, Filtricine, and Protos and a science advisory board member of Genapsys and Jupiter. The other authors declare that they have no competing interests. **Data and materials availability:** All data associated with this study are present in the paper or the Supplementary Materials or have been uploaded to the Flow Repository (http://flowrepository.org/; experiment ID: FR-FCM-Z3FH), Metabolomics Workbench (www.metabolomicsworkbench.org/; project ID: ST001681), and Dryad (Proteome) (http://datadryad.org/ and https://doi.org/10.5061/dryad.280gb5mpd). The newly generated code is available via Zenodo (http://zenodo.org; doi: 10.5281/zenodo.4509768).

Submitted 26 July 2020
Accepted 14 April 2021
Resubmitted 1 December 2020
Published 5 May 2021
10.1126/scitranslmed.abd9898

**Citation:** I. A. Stelzer, M. S. Ghaemi, X. Han, K. Ando, J. J. Hédou, D. Feyaerts, L. S. Peterson, K. K. Rumer, E. S. Tsai, E. A. Ganio, D. K. Gaudillière, A. S. Tsai, B. Choisy, L. P. Gaigne, F. Verdonk, D. Jacobsen, S. Gavasso, G. M. Traber, M. Ellenberger, N. Stanley, M. Becker, A. Culos, R. Fallahzadeh, R. J. Wong, G. L. Darmstadt, M. L. Druzin, V. D. Winn, R. S. Gibbs, X. B. Ling, K. Sylvester, B. Carvalho, M. P. Snyder, G. M. Shaw, D. K. Stevenson, K. Contrepois, M. S. Angst, N. Aghaeepour, B. Gaudillière, Integrated trajectories of the maternal metabolome, proteome, and immunome predict labor onset. *Sci. Transl. Med.* **13**, eabd9898 (2021).

Science Translational Medicine

# Integrated trajectories of the maternal metabolome, proteome, and immunome predict labor onset

Ina A. Stelzer, Mohammad S. Ghaemi, Xiaoyuan Han, Kazuo Ando, Julien J. Hédou, Dorien Feyaerts, Laura S. Peterson, Kristen K. Rumer, Eileen S. Tsai, Edward A. Ganio, Dyani K. Gaudillière, Amy S. Tsai, Benjamin Choisy, Lea P. Gaigne, Franck Verdonk, Danielle Jacobsen, Sonia Gavasso, Gavin M. Traber, Mathew Ellenberger, Natalie Stanley, Martin Becker, Anthony Culos, Ramin Fallahzadeh, Ronald J. Wong, Gary L. Darmstadt, Maurice L. Druzin, Virginia D. Winn, Ronald S. Gibbs, Xuefeng B. Ling, Karl Sylvester, Brendan Carvalho, Michael P. Snyder, Gary M. Shaw, David K. Stevenson, Kévin Contrepois, Martin S. Angst, Nima Aghaeepour and Brice Gaudillière

*Sci Transl Med* **13**, eabd9898.
DOI: 10.1126/scitranslmed.abd9898

**Toward better prediction of labor**

Current methods to predict spontaneous labor are fairly inaccurate. To provide better estimates and biomarkers of labor onset, the biological processes that lead up to labor need to be better understood. Stelzer *et al* . performed metabolome, proteome, and immunome studies on blood samples from 63 women in the 100 days before delivery. They identified a surge in IL-1R4 and steroid hormones in the weeks before delivery, which was coordinated with a switch from immune activation to regulation of inflammatory responses. A model was then constructed to predict time to labor independent of gestational age. These results may be helpful for development of more accurate methods to predict labor.